

1 **Respiromics – an integrative analysis linking mitochondrial**
2 **bioenergetics to molecular signatures**

3

4 Ellen Walheim¹, Jacek R. Wiśniewski², Martin Jastroch^{1*}

5

6 **Running title:** Respiromics

7

8 1. Institute for Diabetes and Obesity, Helmholtz Diabetes Center, Helmholtz Zentrum
9 München, 85764 Neuherberg, Germany

10 2. Biochemical Proteomics Group, Department of Proteomics and Signal Transduction,
11 Max Planck Institute of Biochemistry, Martinsried, Germany

12

13

14 *Corresponding author: Martin Jastroch, martin.jastroch@helmholtz-muenchen.de

15

16 List of abbreviations: DIO, Diet induced obesity; ETC, Electron transport chain; HFD, High fat
17 diet; TPA, Total protein approach

18

19 **Words main text:**

20 **Figures:**

21 **Tables:**

22

23 **Summary**

24 **Objective:** Energy metabolism is challenged upon nutrient stress, eventually leading to a
25 variety of metabolic diseases that represent a major global health burden.

26 **Methods:** Here, we combine quantitative mitochondrial *respirometry* (Seahorse technology) and
27 *proteomics* (LC-MS/MS-based total protein approach) to understand how molecular changes
28 translate to changes in mitochondrial energy transduction during diet-induced obesity (DIO) in
29 the liver.

30 **Results:** The integrative analysis reveals that significantly increased palmitoyl-carnitine
31 respiration is supported by an array of proteins enriching lipid metabolism pathways. Upstream
32 of the respiratory chain, the increased capacity for ATP synthesis during DIO associates
33 strongest to mitochondrial uptake of pyruvate, which is routed towards carboxylation. At the
34 respiratory chain, robust increases of complex I are uncovered by cumulative analysis of single
35 subunit concentrations. Specifically nuclear-encoded accessory subunits, but not mitochondrial-
36 encoded or core units, appear to be permissive for enhanced lipid oxidation.

37 **Conclusion:** Our integrative analysis, that we dubbed “*respiromics*”, represents an effective tool
38 to link molecular changes to functional mechanisms in liver energy metabolism, and, more
39 generally, can be applied for mitochondrial analysis in a variety of metabolic and mitochondrial
40 disease models.

41

42 **Key words:** mitochondria, respirometry, proteomics, mitochondrial pyruvate carrier, liver
43 disease, bioenergetics, obesity, diabetes

44 **1. Introduction**

45 Mitochondria play a central role in energy metabolism as they convert nutrient to cellular energy.
46 In response to physiological and environmental stress, mitochondria require functional
47 adaptation to match increased ATP demand and to maintain metabolic homeostasis [1]. The
48 complex adaptation of the organelle is integrated to assure cellular homeostasis and requires
49 multiple adjustments of signaling pathways and structural proteins. In a homeostatic system,
50 mitochondrial energy flux is balanced by two major processes: the reactions that produce proton
51 motive force at the mitochondrial inner membrane, and the reactions that consume proton
52 motive force to fuel cellular functions [2]. The production of proton motive force depends on the
53 capacity of the respiratory chain, substrate preferences and routes of substrate supply; multiple
54 distinct metabolic pathways regulate the latter. Proton motive force is consumed either by ATP
55 synthesis, or is dissipated as heat by the mitochondrial proton leak [3]. In most cell-types,
56 electron flux is mainly controlled by ATP turnover, but feedback mechanisms communicate also
57 upstream, regulating substrate supply as documented for the liver using top-down and elasticity
58 control analyses of mitochondrial and cellular energy metabolism [4-6]. As cells are always
59 exposed to fluctuations in energy supply and demand, intrinsic flexibility and allosteric control is
60 partially supported by adjustments of protein concentrations. However, in particular chronic
61 impairments of energy balance, such as oversupply (during overnutrition) or the lack of demand
62 (e.g. the lack of exercise), may reach the limits of intrinsic flexibility and allosteric regulation,
63 possibly even the limits of proteomic adaptation, thus establishing pathologies of the metabolic
64 syndrome [7, 8].

65 The enormous complexity of mitochondrial regulation may only be captured using global
66 molecular and functional analyses. Functional bioenergetic adjustments can be monitored
67 overall as mitochondrial oxygen consumption, and partitioning oxygen consumption into
68 functional modules may simplify the metabolic complexity. Respirometry enables to determine

69 oxidative capacity and substrate preferences [9]. Using appropriate respiratory chain inhibitors
70 and activators, oxygen consumption rates are instrumental to indirectly estimate consumers of
71 proton motive force such as ATP synthase activity (state 3 respiration) and proton leak (state 4).
72 In particular state 4 respiration measurements bares pitfalls, as state 4 rates inevitably also
73 depend on substrate oxidation capacity, thus only “estimates” mitochondrial proton conductance
74 [10]. The ratio of state 3/state4, termed respiratory control ratio (RCR), is considered a powerful
75 internally normalized parameter to detect defective mitochondrial properties [9]. Furthermore,
76 RCRs may assist to clarify whether changes of state 4 respiration are changes in proton leak
77 (changing RCR) or in substrate oxidation capacity (maintaining RCR). Chemical uncouplers
78 such as lipophilic acids (e.g. DNP, FCCP) are generally used to remove respiratory control and
79 maximize substrate oxidation. However, the respiratory response is dose-sensitive and
80 deleterious effects of chemical uncouplers could be overseen. Quantitative changes in ATP
81 demand during physiological adaptation are probably best reflected in changes of state 3
82 respiration, which is balanced by substrate supply and ATP demand. Furthermore, state 3 rates
83 are relatively robust by avoiding deleterious effects of non-physiological chemical inhibitors.

84 In the past, bulks of mitochondria were required to measure respiration in single-chambered
85 Clark-type electrodes [11], hampering efforts to examine high sample numbers and various
86 conditions in a timely manner. New technologies such as extracellular flux analyzers in the 24-
87 or 96-well format, also dubbed “Seahorse technology” referring to the initial vendor, have been
88 developed to simultaneously analyze mitochondrial respiration with high sampling sizes in minor
89 quantities [12]. The automated measurements not only enable screening efforts (e.g. for drugs)
90 but also increase the statistical power to detect subtle bioenergetic adjustments, such as those
91 found during physiological adaptation or multi-factorial metabolic diseases. Most of the
92 molecular adjustments are controlled by systemic changes of gene programs rather than of
93 single genes and the complexity hampers our understanding on physiological regulation of
94 mitochondrial energy metabolism. Thus, respiratory changes in response to (patho)physiological

95 challenges cannot easily be attributed to single proteins or entire metabolic networks, while the
96 bioenergetic impact of characterized proteins is assessable by mitochondrial respiration [e.g.
97 13, 14]. To identify novel molecular players or signatures, global proteomics are required.
98 Modern mass spectrometry and the latest approaches in label-free protein quantification enable
99 quantitative proteomic analysis, up to the level of absolute protein concentrations [15]. Without a
100 doubt, the progress in omics-analyses has promoted in-depth understanding of different types of
101 physiological and pathogenic processes. However, the inherent problem of all omic datasets is
102 the vast amount of information (transcripts, proteins, metabolites) that requires processing and
103 filtering in order to reduce the number of protein candidates for further detailed analyses. How
104 stress-related adjustments in the protein network impact cellular function still represents the
105 ultimate question that drives therapeutic target identification for a variety of diseases. To the
106 best of our knowledge, proteomic datasets have mostly been integrated only with other -omics
107 data, such as transcriptomics or metabolomics, in order to characterize complex metabolic
108 phenotypes [e.g. 16]. It is clear, however, that the systematic, unbiased integration of
109 proteomics with functional data would establish a powerful link between the molecular basis and
110 specific cellular functions. Thus, the development of workflows to establish protein-function
111 relationships for energy metabolism in complex systems such as intact mitochondria may
112 benefit the understanding of metabolic and mitochondrial disease paradigms. Recently,
113 proteomics were combined with enzyme kinetics to characterize tissue-specific types of the
114 glycolytic and gluconeogenic pathways [17].

115 In this study, we combine LC-MS/MS-based total protein approach (TPA) with multi-well
116 respiratory flux analysis of isolated mitochondria to link absolute protein concentrations with
117 changes in mitochondrial energy transduction. This integrative analyses aims to identify direct
118 functional and mechanistic interactions to improve our mechanistic understanding how
119 molecular key players and networks impact mitochondrial bioenergetics, and how cellular
120 energy metabolism adapts to stress situations. As proof-of-principle for this integrative workflow,

121 that we dub “respiromics”, we focus on nutrient-stressed energy metabolism in the obese
122 mouse liver, a model of broad medical interest to elucidate how Western lifestyle and excessive
123 food intake promote progression from non-alcoholic fatty liver to hepatosteatosis [18] and the
124 progression from high blood glucose to diabetes.

125 Instead of analyzing isolated datasets of mitochondrial respiration rates and of protein lists, we
126 enhance the mechanistic picture using global correlation analysis. The integrative analysis
127 highlights the mitochondrial pyruvate carrier (MPC) as prime element controlling respiration in
128 the liver. Furthermore, we show that mitochondrial lipid oxidation of DIO mice is specifically
129 enhanced by an array of (partially novel) disease-related proteins controlling catabolism of fatty
130 acids and amino acids. The TPA also enabled to cumulate and quantify multimeric protein
131 complexes. Herein, we found that specifically respiratory complex I is elevated by the sum of
132 nuclear-encoded accessory subunits of complex I, rather than by mitochondrial encoded or core
133 subunits, and associates to enhanced lipid oxidation. This proof-of-principle study shows that
134 “respiromic” analyses are capable to reveal functional sets of stress-induced and disease-
135 related proteins that deserve further investigation as biomarkers or therapeutic targets.

136

137 **2. Materials and Methods**

138 **2.1. Animals**

139 C57/Bl6J mice were housed at room temperature (23°C) in a 12h-light/dark cycle. Starting at the
140 age of six weeks, the mice had ad libitum access to either chow diet (CHOW: Teklad LM-485,
141 17 kcal% fat, 58 kcal% carbohydrate, 25 kcal% protein) or high fat diet (HFD: Surwit Diet
142 D12331, 58 kcal% fat, 25.5 kcal% carbohydrate, 16.4 kcal% protein, Research diets) for 15.5
143 weeks.

144 **2.2. Mitochondrial isolation**

145 Livers were dissected and immediately placed in ice-cold isolation buffer (STE; 250 mM
146 Sucrose, 5 mM TRIS, 2 mM EGTA, pH adjusted to 7.4 at 4°C) for the isolation of mitochondria
147 by differential centrifugation at 4°C. The livers were washed in STE buffer, cut to small pieces,
148 washed several times, and homogenized in STE containing 0.5% fatty acid-free BSA (Sigma
149 No: A3803-50G) using a glass dounce homogenizer. After centrifugation at 800 g for 10 min, the
150 supernatant was filtered and transferred to a fresh tube. The suspension was centrifuged at
151 8000 g for 10 min for sedimentation of the mitochondrial fraction. Excessive residual fat was
152 wiped off the tube walls, and the pellet was resuspended in fresh STE. During the final
153 centrifugation step, the initial speed of 2000 g was increased after 5 min to 4000 g for another 5
154 min. The final pellet was resuspended in a minimal amount of STE buffer and the protein
155 content was quantified using Biuret reagent.

156 **2.3 Mitochondrial respiration**

157 Mitochondrial respiration rates were measured in a XF96 extracellular flux analyzer (Seahorse
158 Bioscience, Billerica). The measuring buffer (MAS) consisted of 70 mM sucrose, 220 mM
159 mannitol, 10 mM KH₂PO₄, 5 mM MgCl₂, 2 mM HEPES, 1 mM EGTA, 0.5% fatty acid-free BSA
160 and the pH was adjusted to 7.2 at 37°C. Mitochondria, respiratory chain substrates and
161 inhibitors were added as follows: 2.5 µg mitochondria per well were incubated with 10 mM

162 succinate and 2 μ M rotenone; 5 μ g mitochondria per well were incubated with 10 mM pyruvate
163 and 3 mM malate, and 10 μ g mitochondria per well were incubated with 50 μ M palmitoyl-
164 carnitine and 3 mM malate. After two initial measurement cycles, ADP was injected at 4 mM
165 (final concentration) and a single measurement cycle recorded. Subsequent injection of 2.5 g/ml
166 oligomycin shifted mitochondria to state 4o (proton leak respiration), injection of 4 μ M FCCP
167 induced maximal substrate oxidation, and 4 μ M antimycin A blocked mitochondrial respiration
168 for baseline correction. Every condition per animal was measured in multiple wells and
169 averaged.

170 **2.4. Complex I activity assay**

171 Complex I activity was measured with a “Complex I Enzyme Activity Microplate Assay Kit
172 (Colorimetric)” (ab109721) from abcam according to the manufacturer’s instructions.

173 **2.5. Protein Digestion and Peptide Fractionation**

174 Sample preparation for mass spectrometry was performed by denaturing liver mitochondria with
175 2% SDS and 100 mM DTT. Protein lysates and extracts containing 100 μ g of total protein were
176 processed in the 30k filtration units (Microcon, Millipore) centrifuged at 10,000 \times g using the
177 MED-FASP protocol [21]. Endoproteinase Lys-C and trypsin were used for sequential digestion
178 of proteins. The enzyme to protein ratios were 1/50. Duplicates of each sample were prepared
179 and analyzed. Protein and peptide concentrations were assayed using the 'WF'-assay [22].

180 **2.6. LC-MS/MS Analysis**

181 Aliquots containing \sim 8 μ g peptide were separated on a reverse phase column (20 cm \times 75 μ m
182 inner diameter) packed with 1.8 μ m C18 particles (Dr. Maisch GmbH, Ammerbuch-Entringen,
183 Germany) using a 3 h acetonitrile gradient in 0.1% formic acid at a flow rate of 250 nl/min. The
184 LC was coupled to a Q Exactive HF mass spectrometer (Thermo Fisher Scientific, Germany) via
185 a nanoelectrospray source (Proxeon Biosystems). The Q Exactive HF was operated in data
186 dependent mode with survey scans of 300-1650 m/z acquired at a resolution of 60,000. Up to
187 the top 15 most abundant isotope patterns with charge m/z \geq 2 from the survey scan were

188 selected with an isolation window of 1.4 Th and fragmented by HCD with normalized collision
189 energies of 25. The maximum ion injection times for the survey scan and the MS/MS scans
190 were 20 ms and 60 ms, respectively. The ion target value for MS1 and MS2 scan modes were
191 set to 3×10^6 and 1×10^5 , respectively. The dynamic exclusion was 30 s. The raw data have been
192 deposited to the ProteomeXchange Consortium [PMID:24727771] via the PRIDE partner
193 repository with the dataset identifier PXD002289 (Reviewer account details:

194 Username: reviewer14529@ebi.ac.uk, Password: dl0046sZ)

195 **2.7. Data Analysis**

196 The MS data was analyzed using the software environment MaxQuant [23] version 1.2.6.20.
197 Proteins were identified by searching of MS and MS/MS data against UniProtKB/Swiss-Prot
198 database (May 2013) containing 50807 sequences. The FDR was derived by analyzing the
199 decoy database. Carbamidomethylation of cysteines was set as a fixed modification. The initial
200 allowed mass deviation of the precursor ion was up to 6 ppm, and for the fragment masses it
201 was up to 20 ppm. The maximum false peptide discovery rate was specified as 0.01. Protein
202 concentrations were calculated on the basis of spectral protein intensity using the Total Protein
203 Approach (TPA)[15] using following equation:

$$Protein\ concentration(i) = \frac{MS_signal(i)}{Total\ MS_signal \times MW(i)} \left[\frac{mol}{g\ total\ protein} \right]$$

204 where MS_signal and Total MS_signal refer to total MS1 signal intensity of the protein i and the
205 total protein MS1 signal.

206 **2.8. Computational filtering for mitochondrial proteins and molecular mass**

207 In order to exclude confounding effects of non-mitochondrial proteins in some analyses, the
208 mitochondrial proteome was computationally filtered for proteins located in mitochondria using
209 the MitoCarta 2.0, a compendium of proteins that are located in mitochondria [24]. The
210 experimental proteome and the Mitocarta collection were compared based on gene-ID (Entrez-
211 ID, retrieved from UniProt [25], April 2016) and gene symbol (including synonyms).

212 Discrepancies of annotations were manually curated by comparing the gene descriptions. The
213 total mass of mitochondrial and non-mitochondrial proteins in the suspension after LC-MS/MS
214 analysis was calculated based on protein masses retrieved from UniProt (March 2016) and the
215 protein concentrations calculated by TPA.

216 **2.9. Gene Set Enrichment Analysis, construction of heatmaps, and network analysis**

217 Gene Set Enrichment Analysis was performed with GSEA 2.2.1 [26] with the gene set versions
218 5.1 of KEGG and GO databases (c2.cp.kegg.v5.1.symbols.gmt, c5.all.v5.1.symbols.gmt). The
219 input for the main paper was filtered for mitochondrial proteins ahead of enrichment analysis,
220 GO terms for cellular compartment were not included but can be generated from the original
221 proteomic data deposited at the ProteomeXchange Consortium. Gene Symbols were used as
222 Chip platform and minimum size for gene sets was set to 5. For all other parameters, the default
223 settings were used.

224 Enrichment analysis for KEGG pathways and GO terms irrespective of group affiliation or
225 protein concentration was performed with Enrichr [27] with the databases of April 2016.

226 Enrichment for disease genes was performed using the “Gene set → diseases” Data mining tool
227 by Fontaine and Andrade-Navarro[28]. The heat map of the 30 top up- and down-regulated
228 proteins was generated with GenePattern [29] using default settings. Protein-protein networks
229 were created using String-db using default settings [30].

230 **2.10. Correlation analysis**

231 State 2, 3, 4o, and 3u respiration rates fueled by palmitoyl-carnitine/malate, pyruvate/malate, or
232 succinate were correlated with every single protein of the mitochondrial proteome and tested for
233 Spearman correlation using JMP 12, as not all protein concentrations follow Gaussian
234 distribution. Respiration rates and complex I activity were correlated with total respiratory
235 complex concentrations by Pearson correlation and linear regression analysis was performed
236 using GraphPad Prism 6.

237 **2.11. Statistical analysis**

238 Statistical analysis was performed using GraphPad Prism 6, JMP 12, and 'Perseus' software
239 (<http://www.biochem.mpg.de/5111810/perseus>). Respiratory data and proteomic data, including
240 summed up concentrations of respiratory complexes, were tested for statistical significance by t-
241 test. Significance of enrichment was calculated by GSEA 2.2.1[26] or Enrichr [27]. Changes in
242 stoichiometry of respiratory complexes were tested for significance by 2-way-ANOVA with Sidak
243 correction for multiple comparisons.

244 **3. Results**

245 **3.1. Obesity increases mitochondrial lipid oxidation in liver mitochondria**

246 High-fat diet feeding for four months induced obesity in mice ($40.1\text{g} \pm 1.0\text{ g}$ body mass, about
247 26% higher than chow-fed controls ($31.8\text{ g} \pm 0.3\text{ g}$; $p < 0.0001$, $n=8$)). Mitochondrial respiration
248 was tested for differences in substrate preferences and oxidation rates (depicted in Fig. 1A).
249 Pyruvate and palmitoyl-carnitine (PC) are catabolized to acetyl-CoA but cannot independently
250 drive tricarboxylic acid (TCA) cycle flux, thus requiring malate as source of oxaloacetate to
251 spark the TCA cycle. Initially, mitochondria were incubated with their respective substrate only
252 (State 2). Then, ADP was injected to induce phosphorylation (State 3), followed by oligomycin to
253 inhibit the ATP synthase (State 4o) and the chemical uncoupler FCCP to induce maximal
254 respiration (State 3u). While neither pyruvate/malate nor succinate-fuelled respiration was
255 significantly affected (Fig. 1B, C), PC respiration rates were increased in response to HFD (Fig.
256 1D). The increased proton leak respiration (state 4o) with PC is not due to increased proton
257 conductance but a result of increased substrate (PC) oxidation. This is corroborated by
258 unchanged RCR (Suppl. Fig. 1) and strong trends towards elevated state 3u respiration
259 ($p=0.0564$). Notably, the mitochondrial adjustments at the functional level still appear subtle,
260 hampering efforts to identify molecular mechanisms. Collectively, we demonstrate that liver
261 mitochondria of HFD-fed mice increase the capacity of ATP production through increased lipid
262 oxidation with minor effects on mitochondrial proton leak (Fig. 1E).

263 **3.2. Quantitative liver mitoproteomics**

264 Mitochondrial suspensions of livers from chow- and HFD-fed mice were analyzed with LC-
265 MS/MS and protein concentrations were calculated using the total protein approach (TPA)
266 method. 3565 proteins were identified, encoded by 3529 different genes (Suppl. Table 1).
267 Classifying proteins with either the Gene Ontology (GO)-term 'Mitochondrion' (Fig. 2A) or with
268 the Mitocarta 2.0 database [24] (Fig. 2B) uncovered about three-fold higher diversity of unique
269 non-mitochondrial proteins than of mitochondrial proteins. However, the TPA method enabled
270 the calculation of cumulative protein mass, verifying the enrichment of absolute mitochondrial
271 protein content by the isolation procedure (Fig. 2A, B). Similar degrees of mitochondrial
272 enrichment are seen in the sum of individual protein concentrations (Suppl. Fig. 2). In order to
273 exclude confounding effects of non-mitochondrial proteins in the following enrichment analyses
274 geared towards mechanistic mitochondrial adjustments, the protein list was filtered using the
275 Mitocarta 2.0 database (Suppl. Table 2). 976 proteins were confirmed as mitochondrial, of which
276 161 were significantly altered by HFD feeding ($p < 0.05$). The heat map (Fig. 2C) illustrates the
277 top 30 significantly induced (upper panel) and reduced (lower panel) protein concentrations in
278 response to HFD. Gene Set Enrichment Analysis using GSEA v2.2.1 [7, 26] was performed on
279 all mitochondrial proteins using KEGG (Kyoto Encyclopedia of Genes and Genomes) and GO
280 databases (based on database version 5.1 in GSEA v2.2.1). The stress-induced recruitment of
281 metabolic pathways, in particular related to lipid metabolism, is substantiated by enrichment of
282 eight KEGG pathways and 38 GO terms for molecular function and biological processes in HFD
283 mitochondria ($p < 0.05$) (Fig. 2D). In contrast, one KEGG pathway and 18 GO terms were
284 significantly depleted ($p < 0.05$) but these were mostly related to processes such as apoptosis,
285 development, localization, and proliferation, that are not directly linked with metabolism (Fig.
286 2D).

287 **3.3. Integration of respiratory and proteomic data**

288 Next, we thought to investigate how changes in mitochondrial oxidative phosphorylation
289 associate to and are controlled by specific mitochondrial proteins. Thus, we integrated
290 substrate-specific respiration rates with absolute concentrations of all identified mitochondrial
291 proteins (n = 976). These were tested against their respective respiration rates by correlation
292 analysis, considering Spearman correlation coefficients as significant with $p < 0.05$ (Suppl. Table
293 3, Suppl. Fig. 3A). Given the absence of changes in proton conductance, we focused on
294 physiological meaningful ATP production/turnover rates, represented by correlations with state 3
295 respiration. The integrative analysis associated 192 of 976 mitochondrial proteins to ATP
296 production/turnover (Fig. 3A, Suppl. Table 3), which were depicted in substrate-specific subsets
297 (Fig. 3A, Suppl. Fig. 3B). Substrate-specific correlations suggest the involvement in the control
298 of specific substrate oxidation rates (pyruvate, succinate or PC). However, proteins correlating
299 with state 3 rates irrespective of substrate would rather suggest control over protein
300 concentration by ATP demand. Strikingly, only the mitochondrial pyruvate carrier subunit 1
301 (MPC1) overlaps with state 3 rates of all substrates. Notably, the influence of HFD stress on
302 mitochondrial pyruvate transport is also recovered in the proteomic approach by significant
303 induction of MPC2, resulting in the significantly elevated sum of MPC subunits (Fig. 3B). While
304 the stoichiometry of the heterodimeric MPC is not clarified yet [31, 32], the proteomic recovery
305 suggests a 1:2 ratio (MPC1/2). Given the strong correlation of MPC1 with all substrates,
306 mitochondrial pyruvate transport appears to be the master regulator balancing the production
307 and consumption of proton motive force. The strong correlation between MPC1 and state 3
308 oxidation of all substrates supports a model of ATP demand controlling mitochondrial pyruvate
309 influx. The proteomic data suggest reduced pyruvate decarboxylation by elevated pyruvate
310 dehydrogenase kinase (PDK1 and PDK2) levels (Fig. 3C) and increased pyruvate carboxylation
311 by increased pyruvate carboxylase (PC) concentration. This would be in line with the model, as
312 pyruvate would be rerouted into ATP-demanding anabolic pathways, such as hepatic

313 gluconeogenesis, a typical driver for pathologically high blood glucose levels. The energetic
314 significance of the MPC-dependent funneling of pyruvate is coherent with recent results
315 reporting the requirement of MPC for liver gluconeogenesis [19, 20]. Noticeably from the cellular
316 bioenergetics point of view, gluconeogenesis assists to dissipate energy of the nutrient-
317 overloaded hepatic system, despite all negative effects of gluconeogenesis in the sequelae of
318 metabolic disease.

319 Concerning increased lipid supply during HFD, enhanced lipid oxidation requires a complex
320 protein network. An array of 155 proteins correlated with lipid-dependent ATP production (Fig
321 3A, Suppl. Fig. 3C). Their link to lipid oxidation is confirmed by KEGG pathway enrichment,
322 elucidating “fatty acid degradation” and “fatty acid metabolism”, alongside with “valine, leucine
323 and isoleucine degradation”, “propanoate metabolism” and “oxidative phosphorylation” (Fig.
324 3D). Similarly, GO term enrichment analysis revealed enrichment for “fatty acid beta oxidation”,
325 “(respiratory) electron transport chain” and “NADH dehydrogenase (activity)” in this set of
326 proteins (see Suppl. Fig. 3D). Notably, strong correlations of proteins with state 3 respiration
327 were not necessarily paralleled with significant protein concentration changes, therefore
328 masking their significance for mitochondrial bioenergetics without integrating functional
329 respirometry. To further filter for nutrient stress-related key proteins from the 155-protein list, we
330 considered only proteins that are significantly elevated by HFD and that correlate with PC
331 respiration only under HFD conditions (Suppl. Table 4). Of 46 proteins specifically associating
332 with PC/malate fueled state 3 respiration in HFD, 19 were significantly increased by HFD
333 feeding, i.e. represent potential HFD stress-induced proteins (Fig. 3E). Functional interaction
334 between 16 out of 19 proteins is supported by string-db analysis (Fig. 3F) [30], including Acads,
335 Cpt2, and Hadha, which are all implicated in inborn errors of lipid metabolism according to
336 disease gene enrichment analysis and/or are demonstrated as regulators of beta oxidation [33];
337 [28, 34]. Thus, integrating functional bioenergetics and proteomics appears instrumental to
338 effectively and potently filter for disease-relevant proteins.

339 **3.4. Complex I concentration controls mitochondrial lipid oxidation in the liver**

340 Next, we analyzed in depth the relation between proteomic changes of the electron transport
341 chain and HFD-induced lipid respiration, based on evidence from correlation and enrichment
342 analyses (Fig 3A, Suppl. Table 3, Suppl. Fig. 3C). We find that all ETF (electron transfer
343 flavoprotein) subunits are increased by HFD feeding, thus contributing to the increased lipid
344 oxidation in HFD (Fig. 4A). During lipid oxidation, however, energy from lipid oxidation is also
345 donated to complex I via NADH [35]. Looking into the relative proportions of respiratory
346 complexes, the TPA approach revealed high abundance of respiratory complexes I and V in
347 liver mitochondria (Fig. 4B). However, the TPA approach also enabled to determine quantitative
348 changes of entire respiratory complexes by summing up absolute subunit concentrations. This
349 analysis enabled the discovery of systemic functional changes that may be blurred by analyzing
350 subtle changes in single proteins (Fig. 4C). Strikingly, HFD feeding significantly increased the
351 cumulative concentration of complex I (about 10%) while other respiratory complexes were
352 unchanged. Consistently with PC/malate-fueled state 3 respiration, complex I activity was also
353 increased and correlated significantly with complex I concentrations (Fig. 4D), thus
354 demonstrating that the cumulative complex I concentration is functionally relevant. Not
355 surprisingly, pyruvate respiration rates also correlate with complex I content (Suppl. Fig. 4A), as
356 decarboxylation of pyruvate and catabolism of acetyl-CoA in the TCA cycle fully donates
357 pyruvate's electrons to NADH and eventually complex I. However, pyruvate respiration was not
358 significantly changed in response to HFD (Fig. 1B). Of the remaining respiratory complexes,
359 only complex IV shows association with PC and pyruvate respiration (Suppl. Fig. 4B-E), but was
360 not significantly elevated in HFD (Fig. 4C). Thus, we conclude that at least the HFD-induced
361 lipid oxidation is facilitated through increased complex I content. Notably, HFD-induced stress
362 imposed only mild impacts on single subunit concentrations of complex I (Suppl. Fig. 5A, B),
363 similar to the remaining respiratory complexes (Suppl. Fig. 5C-F). Pertaining to absolute subunit

364 concentrations, we observed the induction of Ndufs4, Ndufa2, Ndufab10, as well as Ndufv2,
365 which is the only complex I core subunit (Fig. 4E).

366 **3.5. Obesity impacts nuclear- but not mitochondrial-encoded subunit** 367 **concentrations and functional capacity of complex I**

368 Next, we focused on mammalian respiratory complex I, which consists of seven mitochondrial-
369 encoded subunits, while the residual 37 are nuclear-encoded [36, 37]. Summing up
370 mitochondrial- and nuclear-encoded subunit concentrations separately demonstrated that the
371 HFD-induced elevation of entire complex I component concentration is impacted by nuclear-
372 encoded subunits, but not mitochondrial-encoded subunits (Fig. 4F). Importantly, the amount of
373 nuclear-encoded but not mitochondrial-encoded subunits correlated strongly with PC and
374 pyruvate-fueled state 3 respiration (Suppl. Fig. 6A). The impact of nuclear-encoded subunits on
375 mitochondrial respiration was also observed through correlations with complex IV (Suppl. Fig.
376 6C), where nuclear-control of activity is well established [38]. We found no associations
377 regarding nuclear-mitochondrial imbalance on complex III and V (Suppl. Fig. 6B, D). The 14
378 core subunits of complex I are highly conserved and build the catalytic part of complex I, while
379 the 30 accessory or “supernumerary” subunits are under suspect to control assembly,
380 regulation, stability, or protection against oxidative stress [39]. Interestingly, only the sum of
381 accessory complex I subunits, but not of core subunits, was increased upon HFD feeding (Fig.
382 4G) and correlates with PC/malate fueled state 3 respiration (Fig. 4H). Notably, the regulation
383 and function of complex I during obesity is important for some metabolic disease drugs, such as
384 metformin, which is currently in the light of structural analyses concerning complex I [40]. Taken
385 together, these integrative analyses reveal that the increase of nuclear-encoded accessory
386 complex I subunits may be permissive, if not required, for increased lipid oxidation in liver
387 mitochondria of HFD fed mice (Fig. 4I). The plasticity of liver mitochondrial respiration per se
388 appears to be mainly permitted by nuclear regulation of complex I and IV subunits.

389

390

391 **4. Conclusions**

392 Novel technologies such as multi-well, plate-based respirometry and new analytic developments
393 in mass-spectrometric analysis provide powerful tools to increase our mechanistic
394 understanding of physiological functions and disease patterns. Here, we demonstrate that the
395 combination of these technologies and the integrative analysis uncovers direct links between
396 mitochondrial function and its molecular basis, with the potential to establish causal
397 relationships for mechanistic discovery in disease-mechanisms. Importantly, measuring
398 absolute values for respiration and protein concentrations is required to establish a robust
399 association between oxidative function and the mitoproteome. The absolute protein
400 concentration output of the TPA approach enables to overcome subtle single protein changes
401 by summation to functional protein modules, thereby enhancing molecular insights into
402 mechanisms. The respiratory complexes provide the ideal proof-of-principle for this workflow as
403 they are directly related to mitochondrial oxygen consumption and assembled of multiple
404 subunits. We substantiate in physiologically-challenged liver mitochondria that this integrative
405 methodological approach improves the linkage map between cellular energy metabolism and
406 the molecular protein adjustments in disease models. We cannot formally exclude an impact of
407 blood cell mitochondria, as the mice were not perfused prior to liver dissection. However, due to
408 vigorous washing steps, the proportion should be small and differential influence of immune
409 cells was not observed when inspecting inflammation marker of the background proteome. The
410 integrative analysis reveals that the mitochondrial pyruvate carrier associates strongest to
411 mitochondrial energy turnover in the liver, and that elevated mitochondrial lipid oxidation is
412 specifically associated, and possibly facilitated, by nuclear-encoded complex I subunits.
413 First, we confirmed that increased systemic lipid metabolism of HFD feeding and obesity is
414 reflected by the increase of PC-fueled respiratory capacity at the level of isolated liver
415 mitochondria [41, 42]. The increased respiratory rates in the mouse liver are in accordance with

416 data on pre-pathological changes of the human liver before accumulating dysfunctional
417 properties at later stages [18]. Analyzing the mouse liver mitoproteome, we show that HFD
418 induces numerous quantitative changes but the molecular adjustments appear rather subtle
419 when inspecting single protein concentrations, hampering attempts to identify distinct molecular
420 signature changes for mitochondrial respiration. Therefore, we hypothesized that functionally-
421 linked protein subsets are responsible for robust regulation of hepatocyte energy metabolism
422 during overnutrition, prior to chronic stress-induced dysfunction that disturbs protein-function
423 relationships. Indeed, KEGG/GO term-enrichment analyses cluster the majority of upregulated
424 proteins to metabolism, in particular fatty acid oxidation, including carnitine palmitoyltransferase
425 1 (Cpt1, Fig 2C), which is the rate limiting enzyme for the long chain fatty acid transport into
426 mitochondria and mitochondrial beta oxidation [43]. While most of the enrichment data appear
427 to be in accordance with the functional respirometric data, uncertainty remained which
428 proteomic changes control distinct parts of the oxidative phosphorylation machinery.

429 While KEGG pathways and GO terms aim to partition the proteome into functional subsets
430 using a broad collection of various parameters, we attempted to build specific functional links
431 our rationale to directly associate proteins or multimeric complex concentrations with the
432 functional readout “mitochondrial respiration”. Herein, we deliver lists of single protein
433 concentrations correlating with substrate-specific or –unspecific mitochondrial respiration.
434 Strikingly, MPC1 correlates strongest with ATP-linked state 3 respiration, irrespective of
435 substrate. Therefore, mitochondrial pyruvate transport appears as master regulator of
436 mitochondrial energy turnover in the liver, possibly not only controlling substrate supply, but is
437 also being controlled by ATP demand. The model relating MPC to ATP demand is further
438 supported by proteomic data that suggest funneling of pyruvate into gluconeogenesis, a highly
439 energy demanding process. Similar observations were made in the liver of the MPC knockout
440 mouse [19, 20]. Besides the basic understanding of mitochondrial energy metabolism upon
441 physiological challenge, the integrative approach may also assist to detect disease-related

442 mechanisms. By systemically filtering the mitoproteome for proteins related to HFD-induced
443 lipid oxidation, string database analysis connected a single network, which included genes
444 causing inborn errors of lipid oxidation (as depicted in Fig. 3E). The integrative analysis further
445 suggested the involvement of multiple respiratory complex subunits in the response to HFD,
446 particularly complex I subunits. Taking advantage of absolute quantitation by LC-MS/MS-based
447 TPA, total subunit concentrations of respective respiratory complexes was instrumental to
448 substantiate the claim of specific complex I adjustments by HFD feeding, providing compelling
449 evidence for the relation between mitochondrial lipid oxidation and nuclear complex I subunits.
450 Thus, HFD-induced mitochondrial adjustments are controlled via nucleus-mitochondrion
451 communication rather than being mitochondrion-autonomous, affecting nuclear transcription and
452 translation. The imbalance in mito-nuclear regulation during HFD feeding may foster cellular
453 stress and disease as shown for mismatching mitochondrial and nuclear genotypes [44]. In the
454 case of aging muscle, nuclear-mitochondrial communication was reported to be mediated by
455 declining NAD⁺ in the nucleus, reversible, and PGC-1alpha/beta-independent [45]. In further
456 expansion to this study, the integration of global nuclear gene regulation may be feasible to
457 understand which factors wire mitochondrial biology to nuclear control.
458 Taken together, the integration of mitochondrial functional analysis and quantitative proteomic
459 analysis is suitable for revealing molecular signatures controlling energetic adjustments in diet-
460 induced obesity, providing a tool to explore proteins that impact mitochondrial respiration and
461 substrate preferences in disease, physiological and environmental challenges.

462

463 **Acknowledgements**

464 We thank Ms Katharina Zettl for excellent technical assistance, Ms Silke Morin and Dr. Susanne
465 Keipert for editing of the manuscript. This work was supported by funding in part to M.J. from
466 the German Diabetes Center (DZD) and in part to J.W. from the Max-Planck-Society (MPS).

467

468 **Author contributions**

469 E.W. performed and analyzed all mitochondrial bioenergetics and bioinformatics experiments; J.
470 W. performed and analyzed proteomics, TPA calculations, and gave advice on experimental
471 design and the manuscript; M.J. conceptualized and supervised the research plan, and assisted
472 in mitochondrial bioenergetics experiments; E.W. and M.J. interpreted all data and wrote the
473 manuscript.

474 **Competing financial interest**

475 The authors declare no competing financial interests.

476

477 **References**

- 478 [1] M.D. Brand, The efficiency and plasticity of mitochondrial energy transduction, *Biochem Soc Trans*,
479 33 (2005) 897-904.
- 480 [2] P. Mitchell, Coupling of phosphorylation to electron and hydrogen transfer by a chemi-osmotic type
481 of mechanism, *Nature*, 191 (1961) 144-148.
- 482 [3] M. Jastroch, A.S. Divakaruni, S. Mookerjee, J.R. Treberg, M.D. Brand, Mitochondrial proton and
483 electron leaks, *Essays Biochem*, 47 (2010) 53-67.
- 484 [4] S. Soboll, M.-H. Oh, G.C. Brown, Control of oxidative phosphorylation, gluconeogenesis, ureagenesis
485 and ATP turnover in isolated perfused rat liver analyzed by top-down metabolic control analysis,
486 *European Journal of Biochemistry*, 254 (1998) 194-201.
- 487 [5] D.F.S. Rolfe, M.D. Brand, Proton leak and control of oxidative phosphorylation in perfused, resting
488 rat skeletal muscle, *Biochimica et Biophysica Acta (BBA) - Bioenergetics*, 1276 (1996) 45-50.
- 489 [6] G.C. Brown, P.L. Lakin-Thomas, M.D. Brand, Control of respiration and oxidative phosphorylation in
490 isolated rat liver cells, *European Journal of Biochemistry*, 192 (1990) 355-362.
- 491 [7] V.K. Mootha, C.M. Lindgren, K.-F. Eriksson, A. Subramanian, S. Sihag, J. Lehar, P. Puigserver, E.
492 Carlsson, M. Ridderstrale, E. Laurila, N. Houstis, M.J. Daly, N. Patterson, J.P. Mesirov, T.R. Golub, P.
493 Tamayo, B.M. Spiegelman, E.S. Lander, J.N. Hirschhorn, D. Altshuler, L.C. Groop, PGC-1 α -
494 responsive genes involved in oxidative phosphorylation are coordinately downregulated in human
495 diabetes, *Nature Genetics*, 34 (2003) 267-273.
- 496 [8] K. Morino, K.F. Petersen, S. Dufour, D. Befroy, J. Frattini, N. Shatzkes, S. Neschen, M.F. White, S.
497 Bilz, S. Sono, M. Pypaert, G.I. Shulman, Reduced mitochondrial density and increased IRS-1 serine
498 phosphorylation in muscle of insulin-resistant offspring of type 2 diabetic parents, *The Journal of Clinical*
499 *Investigation*, 115 (2005) 3587-3593.
- 500 [9] M.D. Brand, D.G. Nicholls, Assessing mitochondrial dysfunction in cells, *Biochemical Journal*, 435
501 (2011) 297-312.
- 502 [10] A.S. Divakaruni, M.D. Brand, The Regulation and Physiology of Mitochondrial Proton Leak,
503 *Physiology*, 26 (2011) 192-205.
- 504 [11] L.C.J. Clark, MONITOR AND CONTROL OF BLOOD AND TISSUE OXYGEN TENSIONS,
505 *ASAIO Journal*, 2 (1956) 41-48.
- 506 [12] G.W. Rogers, M.D. Brand, S. Petrosyan, D. Ashok, A.A. Elorza, D.A. Ferrick, A.N. Murphy, High
507 throughput microplate respiratory measurements using minimal quantities of isolated mitochondria, *PLoS*
508 *one*, 6 (2011) e21746.
- 509 [13] B. Faubert, E.E. Vincent, T. Griss, B. Samborska, S. Izreig, R.U. Svensson, O.A. Mamer, D.
510 Avizonis, D.B. Shackelford, R.J. Shaw, R.G. Jones, Loss of the tumor suppressor LKB1 promotes
511 metabolic reprogramming of cancer cells via HIF-1 α , *Proceedings of the National Academy of Sciences*,
512 111 (2014) 2554-2559.

- 513 [14] X. Nie, M. Li, B. Lu, Y. Zhang, L. Lan, L. Chen, J. Lu, Down-Regulating Overexpressed Human
514 Lon in Cervical Cancer Suppresses Cell Proliferation and Bioenergetics, *PloS one*, 8 (2013) e81084.
- 515 [15] J.R. Wisniewski, D. Rakus, Multi-enzyme digestion FASP and the 'Total Protein Approach'-based
516 absolute quantification of the *Escherichia coli* proteome, *Journal of proteomics*, 109 (2014) 322-331.
- 517 [16] Y. Wu, Evan G. Williams, S. Dubuis, A. Mottis, V. Jovaisaite, Sander M. Houten, Carmen A.
518 Argmann, P. Faridi, W. Wolski, Z. Kutalik, N. Zamboni, J. Auwerx, R. Aebersold, Multilayered Genetic
519 and Omics Dissection of Mitochondrial Activity in a Mouse Reference Population, *Cell*, 158 (2014)
520 1415-1430.
- 521 [17] J.R. Wiśniewski, A. Gizak, D. Rakus, Integrating Proteomics and Enzyme Kinetics Reveals Tissue-
522 Specific Types of the Glycolytic and Gluconeogenic Pathways, *Journal of Proteome Research*, 14 (2015)
523 3263-3273.
- 524 [18] C. Koliaki, J. Szendroedi, K. Kaul, T. Jelenik, P. Nowotny, F. Jankowiak, C. Herder, M. Carstensen,
525 M. Krausch, Wolfram T. Knoefel, M. Schlessak, M. Roden, Adaptation of Hepatic Mitochondrial
526 Function in Humans with Non-Alcoholic Fatty Liver Is Lost in Steatohepatitis, *Cell Metabolism*, 21
527 (2015) 739-746.
- 528 [19] Kyle S. McCommis, Z. Chen, X. Fu, William G. McDonald, Jerry R. Colca, Rolf F. Kletzien,
529 Shawn C. Burgess, Brian N. Finck, Loss of Mitochondrial Pyruvate Carrier 2 in the Liver Leads to
530 Defects in Gluconeogenesis and Compensation via Pyruvate-Alanine Cycling, *Cell metabolism*, 22
531 (2015) 682-694.
- 532 [20] Lawrence R. Gray, Mst R. Sultana, Adam J. Rauckhorst, L. Oonthonpan, Sean C. Tompkins, A.
533 Sharma, X. Fu, R. Miao, Alvin D. Pawa, Kathryn S. Brown, Erin E. Lane, A. Dohlman, D. Zepeda-
534 Orozco, J. Xie, J. Rutter, Andrew W. Norris, James E. Cox, Shawn C. Burgess, Matthew J. Potthoff,
535 Eric B. Taylor, Hepatic Mitochondrial Pyruvate Carrier 1 Is Required for Efficient Regulation of
536 Gluconeogenesis and Whole-Body Glucose Homeostasis, *Cell Metabolism*, 22 (2015) 669-681.
- 537 [21] J.R. Wisniewski, M. Mann, Consecutive proteolytic digestion in an enzyme reactor increases depth
538 of proteomic and phosphoproteomic analysis, *Analytical chemistry*, 84 (2012) 2631-2637.
- 539 [22] J.R. Wisniewski, F.Z. Gaugaz, Fast and sensitive total protein and Peptide assays for proteomic
540 analysis, *Analytical chemistry*, 87 (2015) 4110-4116.
- 541 [23] J. Cox, M. Mann, MaxQuant enables high peptide identification rates, individualized p.p.b.-range
542 mass accuracies and proteome-wide protein quantification, *Nat Biotechnol*, 26 (2008) 1367-1372.
- 543 [24] S.E. Calvo, K.R. Clauser, V.K. Mootha, MitoCarta2.0: an updated inventory of mammalian
544 mitochondrial proteins, *Nucleic acids research*, 44 (2016) D1251-D1257.
- 545 [25] T.U. Consortium, UniProt: a hub for protein information, *Nucleic acids research*, 43 (2015) D204-
546 D212.
- 547 [26] A. Subramanian, P. Tamayo, V.K. Mootha, S. Mukherjee, B.L. Ebert, M.A. Gillette, A. Paulovich,
548 S.L. Pomeroy, T.R. Golub, E.S. Lander, J.P. Mesirov, Gene set enrichment analysis: A knowledge-based
549 approach for interpreting genome-wide expression profiles, *Proceedings of the National Academy of
550 Sciences*, 102 (2005) 15545-15550.

551 [27] E.Y. Chen, C.M. Tan, Y. Kou, Q. Duan, Z. Wang, G.V. Meirelles, N.R. Clark, A. Ma'ayan, Enrichr:
552 interactive and collaborative HTML5 gene list enrichment analysis tool, BMC Bioinformatics, 14 (2013)
553 128.

554 [28] M.A. Andrade-Navarro, J.F. Fontaine, Gene set to Diseases: disease enrichment analysis on human
555 gene sets with literature data. Genomics and Computational Biology 2, e33 (2016).

556 [29] M. Reich, T. Liefeld, J. Gould, J. Lerner, P. Tamayo, J.P. Mesirov, GenePattern 2.0, Nat Genet, 38
557 (2006) 500-501.

558 [30] D. Szklarczyk, A. Franceschini, S. Wyder, K. Forslund, D. Heller, J. Huerta-Cepas, M. Simonovic,
559 A. Roth, A. Santos, K.P. Tsafou, M. Kuhn, P. Bork, L.J. Jensen, C. von Mering, STRING v10: protein-
560 protein interaction networks, integrated over the tree of life, Nucleic acids research, 43 (2015) D447-
561 D452.

562 [31] D.K. Bricker, E.B. Taylor, J.C. Schell, T. Orsak, A. Boutron, Y.-C. Chen, J.E. Cox, C.M. Cardon,
563 J.G. Van Vranken, N. Dephoure, C. Redin, S. Boudina, S.P. Gygi, M. Brivet, C.S. Thummel, J. Rutter, A
564 Mitochondrial Pyruvate Carrier Required for Pyruvate Uptake in Yeast, Drosophila, and Humans,
565 Science, 337 (2012) 96-100.

566 [32] S. Herzig, E. Raemy, S. Montessuit, J.-L. Veuthey, N. Zamboni, B. Westermann, E.R.S. Kunji, J.-C.
567 Martinou, Identification and Functional Expression of the Mitochondrial Pyruvate Carrier, Science, 337
568 (2012) 93-96.

569 [33] P. Rinaldo, D. Matern, M.J. Bennett, Fatty Acid Oxidation Disorders, Annual Review of Physiology,
570 64 (2002) 477-502.

571 [34] R.S. Rector, R.M. Payne, J.A. Ibdah, Mitochondrial Trifunctional Protein Defects: Clinical
572 Implications and Therapeutic Approaches, Advanced drug delivery reviews, 60 (2008) 1488-1496.

573 [35] R. Oelkrug, M. Kutschke, C.W. Meyer, G. Heldmaier, M. Jastroch, Uncoupling protein 1 decreases
574 superoxide production in brown adipose tissue mitochondria, J Biol Chem, 285 (2010) 21961-21968.

575 [36] J. Hirst, J. Carroll, I.M. Fearnley, R.J. Shannon, J.E. Walker, The nuclear encoded subunits of
576 complex I from bovine heart mitochondria, Biochimica et Biophysica Acta (BBA) - Bioenergetics, 1604
577 (2003) 135-150.

578 [37] E. Balsa, R. Marco, E. Perales-Clemente, R. Szklarczyk, E. Calvo, Manuel O. Landázuri, José A.
579 Enríquez, NDUFA4 Is a Subunit of Complex IV of the Mammalian Electron Transport Chain, Cell
580 Metabolism, 16 (2012) 378-386.

581 [38] R.O. Poyton, J.E. McEwen, Crosstalk Between Nuclear and Mitochondrial Genomes, Annual
582 Review of Biochemistry, 65 (1996) 563-607.

583 [39] K.R. Vinothkumar, J. Zhu, J. Hirst, Architecture of mammalian respiratory complex I, Nature, 515
584 (2014) 80-84.

585 [40] Hannah R. Bridges, Andrew J.Y. Jones, Michael N. Pollak, J. Hirst, Effects of metformin and other
586 biguanides on oxidative phosphorylation in mitochondria, Biochemical Journal, 462 (2014) 475-487.

- 587 [41] P.M. Marvyn, R.M. Bradley, E.B. Mardian, K.A. Marks, R.E. Duncan, Data on oxygen consumption
588 rate, respiratory exchange ratio, and movement in C57BL/6J female mice on the third day of consuming a
589 high-fat diet, *Data in Brief*, 7 (2016) 472-475.
- 590 [42] T.L. Martin, T. Alquier, K. Asakura, N. Furukawa, F. Preitner, B.B. Kahn, Diet-induced Obesity
591 Alters AMP Kinase Activity in Hypothalamus and Skeletal Muscle, *Journal of Biological Chemistry*, 281
592 (2006) 18933-18941.
- 593 [43] J.M. Orellana-Gavaldà, L. Herrero, M.I. Malandrino, A. Pañeda, M. Sol Rodríguez-Peña, H. Petry,
594 G. Asins, S. Van Deventer, F.G. Hegardt, D. Serra, Molecular therapy for obesity and diabetes based on a
595 long-term increase in hepatic fatty-acid oxidation, *Hepatology*, 53 (2011) 821-832.
- 596 [44] A. Latorre-Pellicer, R. Moreno-Loshuertos, A.V. Lechuga-Vieco, F. Sanchez-Cabo, C. Torroja, R.
597 Acin-Perez, E. Calvo, E. Aix, A. Gonzalez-Guerra, A. Logan, M.L. Bernad-Miana, E. Romanos, R. Cruz,
598 S. Cogliati, B. Sobrino, A. Carracedo, A. Perez-Martos, P. Fernandez-Silva, J. Ruiz-Cabello, M.P.
599 Murphy, I. Flores, J. Vazquez, J.A. Enriquez, Mitochondrial and nuclear DNA matching shapes
600 metabolism and healthy ageing, *Nature*, 535 (2016) 561-565.
- 601 [45] Ana P. Gomes, Nathan L. Price, Alvin J.Y. Ling, Javid J. Moslehi, M.K. Montgomery, L. Rajman,
602 James P. White, João S. Teodoro, Christiane D. Wrann, Basil P. Hubbard, Evi M. Mercken, Carlos M.
603 Palmeira, R. de Cabo, Anabela P. Rolo, N. Turner, Eric L. Bell, David A. Sinclair, Declining NAD⁺
604 Induces a Pseudohypoxic State Disrupting Nuclear-Mitochondrial Communication during Aging, *Cell*,
605 155 (2013) 1624-1638.
606
607

608

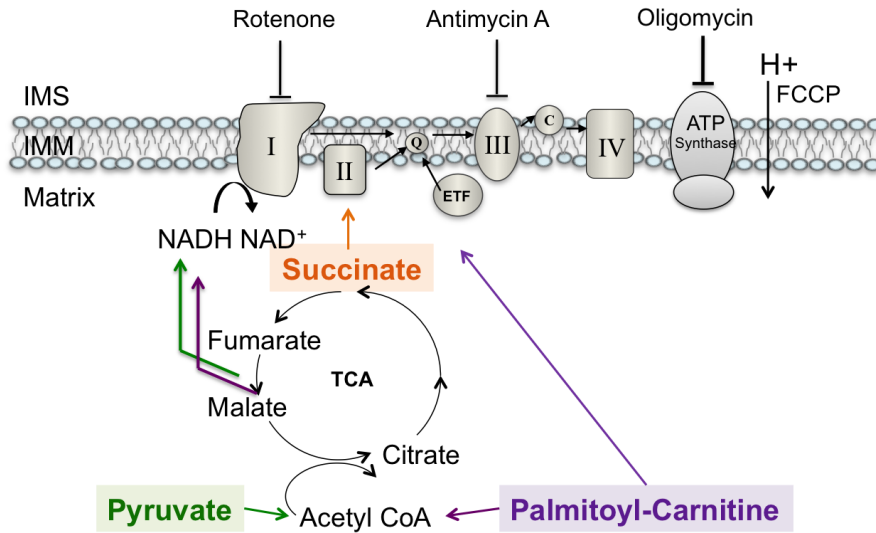
609

610

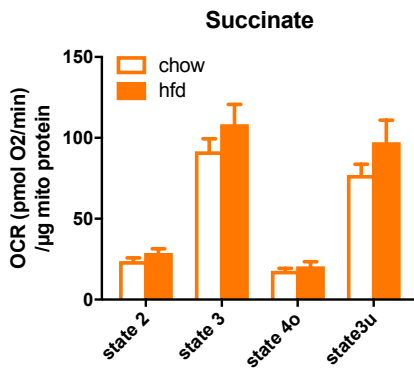
Figures

Figure 1: Respirometry of isolated liver mitochondria from chow vs HFD fed mice. (A) The scheme depicts distinct substrate entry points into the respiratory chain. State 2 (substrate only), state 3 (phosphorylating respiration in presence of ADP), state 4o (ATP synthase inhibited by oligomycin), and state 3u (uncoupled respiration) were corrected for non-mitochondrial oxygen consumption using antimycin A. Respiration rates with (B) pyruvate/malate, (C) palmitoyl-carnitine/malate, and (D) succinate were normalized to mitochondrial protein concentrations. (E) Mitochondrial energy transduction is controlled by substrates entering the electron transport chain (ETC) produce proton motive force (ψ) which can be used for either ATP production or proton leak activity. In HFD liver mitochondria, lipid oxidation is enhanced. Data are expressed as mean \pm SEM; n=8 animals per group, *p<0.05, **p<0.01 by t-test comparing HFD vs chow.

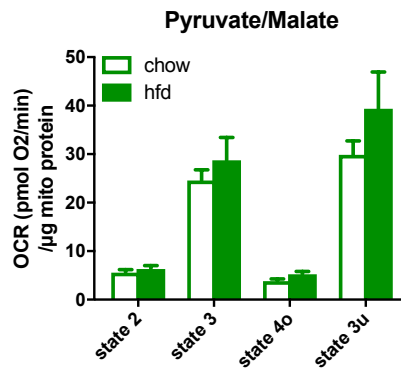
A Mitochondrial energy transduction



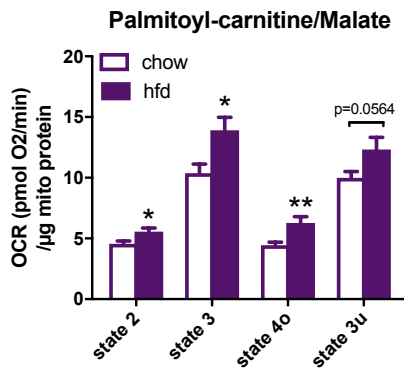
B



C



D



E

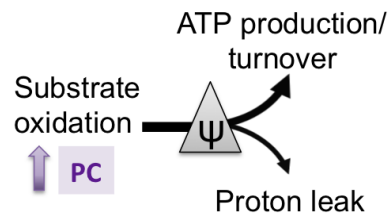


Figure 2: HFD-induced changes of the liver mitochondrial proteome. (A-B) The numeric and mass proportion of mitochondrial protein within the isolated suspension was summed using mitochondrial annotation (A) of the GO database or (B) of the Mitocarta 2.0 database. Specific protein masses were assessed by multiplying protein concentrations x respective molecular masses retrieved from the UniProt database. (C-D) Gene Set Enrichment Analysis [26] was performed with the mitochondrial protein subset defined by Mitocarta 2.0. (C) The heatmap illustrates top 30 significantly up- and downregulated proteins of the HFD group sorted by fold change. For each protein, the relative concentration compared to its mean concentration is colour-coded on a scale from minimum (blue) to maximum (red) concentration for each sample. (D) KEGG pathways (upper panels) and GO-terms (lower panels) of significantly depleted (blue, left panels) or enriched (red, right panels) in response to HFD feeding.

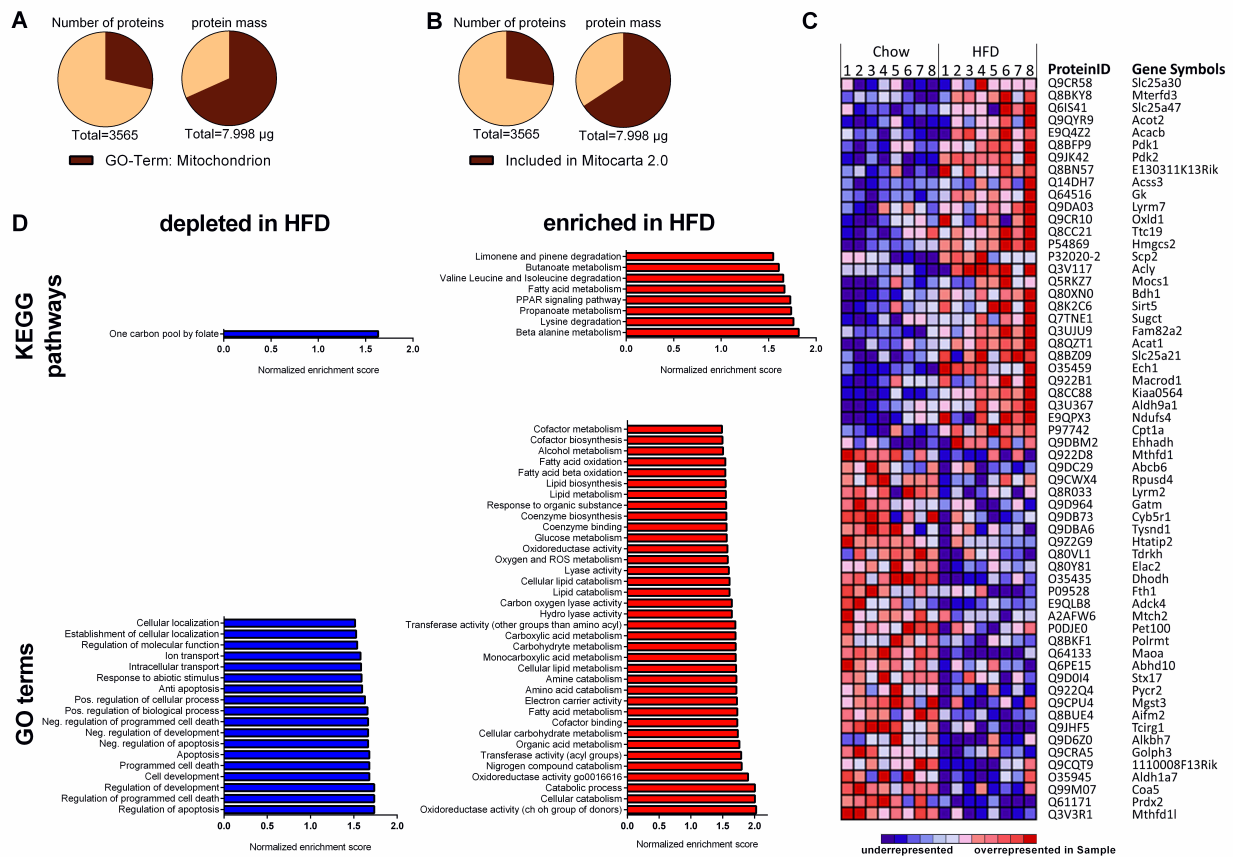
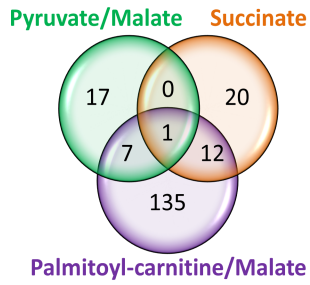
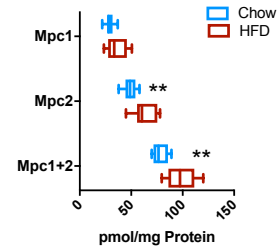


Figure 3: Correlation analysis of mitochondrial respiration and proteome. (A) 976 mitochondrial proteins (as annotated in the Mitocarta 2.0) were correlated with state 3 respiration for different substrates. The numbers in the Venn-diagram depict significantly correlating proteins (Spearman $\rho \geq 0.5$, $p < 0.05$). The single protein correlating with all substrates is MPC1. (B) Absolute protein concentrations of Mpc1, Mpc2 and Mpc1+Mpc2. (C) Routing of mitochondrial pyruvate during HFD-feeding based on proteomic data. Enhanced imported pyruvate is not decarboxylated, as increased levels of pyruvate dehydrogenase kinases PDK1 and PDK2 inhibit pyruvate dehydrogenase (PDH). Increased pyruvate carboxylase (PC) levels support enhanced pyruvate carboxylation, forming oxaloacetate for gluconeogenesis, a highly ATP-demanding process driving respiration. (D) Enrichment analysis for KEGG pathways was performed for proteins significantly correlating with state 3 palmitoyl-carnitine (PC)/malate respiration. The top 10 significantly enriched KEGG pathways are displayed with their respective combined score calculated by Enrichr. (E) Prediction of proteins controlling lipid respiration in response to nutrient stress. Protein levels significantly induced by HFD ($p < 0.05$) were filtered specifically for correlation with HFD-induced PC/malate state 3 respiration. (F) The functional link between HFD-stress induced proteins is strongly supported by the string-db network [30]. Acads, Cpt2, Hadha (indicated by red circle) were previously identified as disease genes for inborn errors of lipid metabolism [28]. All data represent $n=8$ animals. Boxplots indicate 25-75 percentiles, with the vertical line indicating the median and whiskers from minimum to maximum (B) or as mean \pm standard error of mean (C). * $p < 0.05$, ** $p < 0.01$, *** $p < 0.001$, **** $p < 0.0001$ in a t-test comparing chow vs HFD.

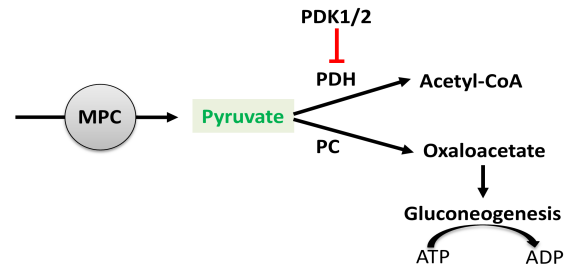
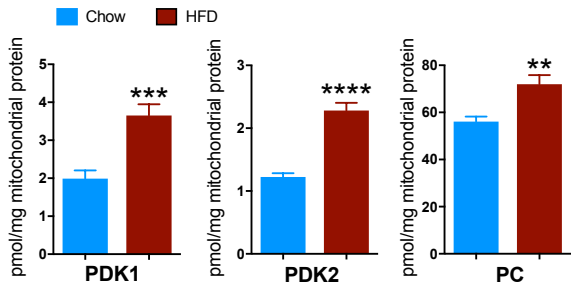
A Venn diagram of state 3 - associated proteome



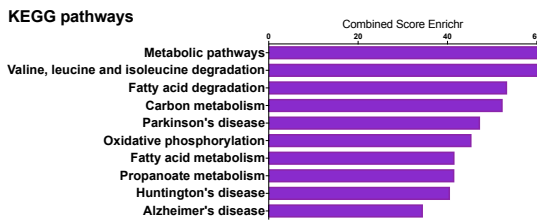
B Mitochondrial pyruvate carrier (Mpc)



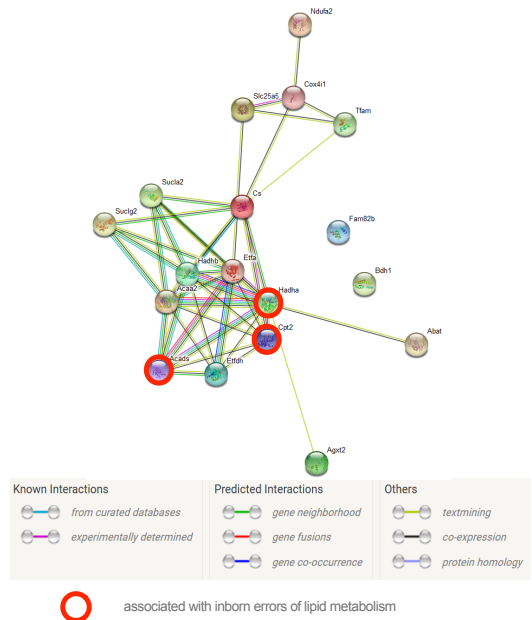
C Routing of mitochondrial pyruvate



D Pathways controlling lipid oxidation



F Network related to HFD-induced respiration



E HFD-stress induced lipid oxidation

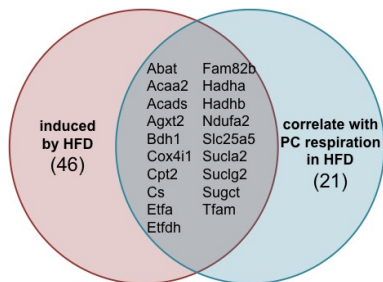


Figure 4: HFD-induced lipid oxidation is facilitated by increased complex I content and activity, regulated by nuclear accessory subunits. (A) Scheme showing palmitoyl-carnitine entry into the electron transport chain (ETC). Electron transfer flavoprotein (ETF) subunits are increased in HFD-liver mitochondria. (B) The pie chart shows relative proportion of each complex of the ETC. Single subunit concentrations were summed up for each respiratory complex. (C) Total cumulative concentration of respective ETC complex subunits, depicted as group mean values. Asterisk indicates significantly increased complex I concentration in HFD. (D) Respiratory complex I activity by colorimetric assay (bar chart). Cumulated complex I concentrations correlate significantly with complex I activity (red) and PC-state 3 respiration (purple). (E) The absolute concentrations of complex I subunits that are significantly changed by HFD (see Fig. S5 for the complete list of absolute subunit concentrations). (F) The additive concentration of nuclear-encoded complex I subunits (left panel) is increased by HFD, while mitochondrial-encoded subunits are not (right panel). (G) The cumulative concentrations of complex I core and accessory subunits were correlated with (H) PC-state 3 respiration. (I) The integrative analysis of respirometry and proteomics supports model of bioenergetic adaptation in response to HFD that permits increasing lipid oxidation by upregulation of nuclear-encoded accessory complex I subunits. All data represent n=8 animals. Boxplots indicate 25-75 percentiles, with the vertical line indicating the median and whiskers from minimum to maximum (A, E) or as mean \pm standard error of mean. * $p < 0.05$, ** $p < 0.01$ comparing chow vs HFD by t-test (A, C, D, E, F, G). (D, H) R^2 and p-value of Pearson-correlation are given, linear regression is shown where Pearson-correlation is significant ($p < 0.05$).

